A singlet/triplet Josephson junction on a substrate

Kaito Yamaki and Yasuhiro Asano
Department of Applied Physics, Hokkaido University, Sapporo 060-8628, Japan
(Dated: May 16, 2025)

We discuss the Josephson effect in a spin-singlet superconductor/spin-triplet superconductor junction fabricated on a substrate. Due to breaking inversion symmetry on the top of the substrate, Rashba spin-orbit interaction works on electrons in the superconductors. As a result, spin-triplet (spin-singlet) Cooper pairs are induced in a spin-singlet (spin-triplet) superconductor. The presence of such induced Cooper pairs enables the lowest order Josephson coupling between the two superconductors. Based on the theoretical results and the recent experimental findings [X. Xu et. al., Phys. Rev. Lett. **132**, 056001 (2024)], we analyze the pair potential of β-$\mathrm{Bi_2Pd}$.

I. INTRODUCTION

Symmetries of the pair potentials in superconductors are usually classified into either spin-singlet even-parity class or spin-triplet odd-parity class. Although spin-singlet superconductivity has been observed in various materials such as mono-element metals and high-T_c cuprates, spin-triplet superconductors (SCs) are very rare. A topological-material-based compound $\mathrm{Cu}_x\mathrm{Bi_2Se_3}$ and several uranium compounds such as $\mathrm{UPt_3}$, $\mathrm{UBe_{13}}$, $\mathrm{UGe_2}$, and $\mathrm{UTe_2}$ are candidates of spin-triplet SCs [1–7]. At present, however, spin-triplet superconductivity in these materials are still under debate. The search for spin-triplet SCs has been an important issue these days in order to realize the quantum computation using non-Abelian statistics of Majorana Fermions. Under such situation, theoretical studies have proposed the recipes of artificial spin-triplet SCs [8–11].

When a new candidate material is synthesized, several experiments are performed to confirm spin-triplet superconductivity. Critical magnetic fields beyond the Pauli limit and unchanged spin susceptibility across T_c are typical signatures of a spin-triplet SC. Experiments in normal-metal/superconductor (NS) proximity structures also tell us the sign of spin-triplet superconductivity such as zero-bias anomaly in the conductance spectra at a T-shaped junction [12, 13] and unusual surface impedance in an NS bilayer [14]. Such characteristic properties of a spin-triplet SC originates from a $\boldsymbol{d}$-vector (the order parameter of spin-triplet superconductivity). In ^{3}He-B phase, for example, $\boldsymbol{d} \propto k_x\boldsymbol{e}_x + k_y\boldsymbol{e}_y + k_z\boldsymbol{e}_z$ is isotropic in both momentum and spin spaces, where $\boldsymbol{e}_j$ with $j = x, y$, and z are the unite vector in spin space in the j direction. As a result, the spin susceptibility becomes isotropic in real space [20]. A $\boldsymbol{d}$-vector proportional to $(k_x + ik_y)$ breaks time-reversal symmetry and generates the intrinsic angular momentum in ^{3}He-A phase. Superconductivity in a heavy fermion compound $\mathrm{UTe_2}$ may be described by a multi-component $\boldsymbol{d}$-vector breaking time-reversal symmetry. [21] Thus, the analyzing the $\boldsymbol{d}$ in a spin-triplet SC is the most important issue in experimental research. In particular, observing the π-phase shift in a superconducting quantum interference device (SQUID) proposed by Geshkenbein, Larkin and Barone (GLB) suggests convincingly spin-triplet superconductivity. [15] Indeed, based on the observed π-phase shift, a recent experiment [16] concludes spin-triplet superconductivity in a topologically nontrivial SC β-$\mathrm{Bi_2Pd}$.[17–19]

In a spin-singlet superconductor/spin-triplet superconductor junction (referred to as a singlet/triplet junction below), the lowest order coupling is absent due to the mismatch of the pair potentials in spin space. Namely, spin dependent potentials are necessary to have the lowest order Josephson coupling in a singlet/triplet junction. Unfortunately GLB did not discuss how the symmetry mismatches are resolved in realistic junctions. Spin-orbit interaction (SOI) at the junction interface [22] is a possible source that enables the lowest order coupling in a singlet/triplet junction. However, as we will show in Sec. V, the interface SOI does not explain the π-phase shift in a SQUID.

In this paper, we study the effects of the Rashba SOI on the Josephson current in a singlet/triplet junction fabricated on a substrate. The Rashba SOI generates a spin-triplet pairing correlation in a spin-singlet superconductor and spin-singlet pairing correlations in a spin-triplet superconductor. Such induced pairing correlations cause the lowest order coupling in a singlet/triplet junction. In addition, the π-phase shift observed in a SQUID can be explained consistently with the selection rules derived from the Rashba SOI. We discuss symmetry of the pair potential in β-$\mathrm{Bi_2Pd}$ with taking the selection rules into account.

This paper is organized as follows. We explain our theoretical model in Sec. II. The analytical expression of the Josephson current is presented in Sec. III. The selection rules for the Josephson coupling are discussed in Sec. IV. We analyze the pairing symmetry in β-$\mathrm{Bi_2Pd}$ in Sec. V. The conclusion is given in Sec. VI. We use the unit of $k_B = \hbar = c = 1$, where k_B is the Boltzmann constant and c is the speed of light.

II. MODEL

Let us consider a singlet/triplet Josephson junction as shown in Fig. 1. Two superconducting thin films are fabricated on a substrate and form a Josephson junction

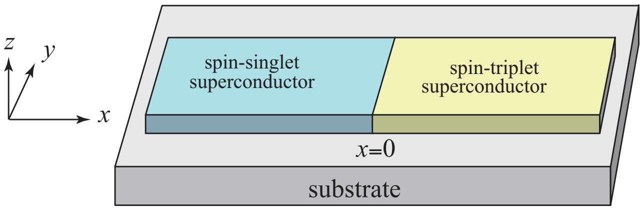

FIG. 1. Schematic picture of a spin-singlet superconductor/spin-triplet superconductor junction which is referred to as a single/triplet junction in the present paper. The current flows in the x direction and the junction interface is at $x = 0$. The cross section of the junction is S.

at $x = 0$. The normal state Hamiltonian in a uniform superconductor is given by

$$\hat{H}_{\mathrm{N}}(j, \boldsymbol{k}) = \xi_{j,\boldsymbol{k}} - \boldsymbol{\alpha}_{\boldsymbol{k}} \cdot \hat{\boldsymbol{\sigma}}, \tag{1}$$

$$\boldsymbol{\alpha}_{\boldsymbol{k}} = (-\lambda k_y, \lambda k_x, 0), \tag{2}$$

$$\xi_{j,\boldsymbol{k}} = \frac{\boldsymbol{k}^2}{2m_j} + \epsilon_j - \mu, \tag{3}$$

where μ is the chemical potential, $\hat{\sigma}_i$ for $i = x, y$, and z is the Paul matrices in spin space. The effective mass of an electron and the energy shift are the material parameters. They are given by $m_j = m_s$ and $\epsilon_j = \epsilon_s$ in a singlet SC, and $m_j = m_t$ and $\epsilon_j = \epsilon_t$ in a triplet SC. As inversion symmetry is broken along the z direction, Rashba spin-orbit interaction (SOI) acts on electrons in thin SCs on a substrate. The pair potential in a spin-singlet SC is described as

$$\hat{\Delta}(s, \boldsymbol{k}) = \Delta_{\boldsymbol{k}}\, i\hat{\sigma}_y\, e^{i\varphi_s}, \quad \Delta_{-\boldsymbol{k}} = \Delta_{\boldsymbol{k}}, \tag{4}$$

where φ_s is the phase of the superconducting condensate. The pair potential in a spin-triplet SC is given by

$$\hat{\Delta}(t, \boldsymbol{k}) = i\boldsymbol{d}_{\boldsymbol{k}} \cdot \hat{\boldsymbol{\sigma}}\, \hat{\sigma}_y\, e^{i\varphi_t}, \quad \boldsymbol{d}_{-\boldsymbol{k}} = -\boldsymbol{d}_{\boldsymbol{k}}, \tag{5}$$

where φ_t is the phase and a three-component vector $\boldsymbol{d}_{\boldsymbol{k}}$ describes spin-triplet superconductivity. Throughout this paper, we consider unitary states, (i. e., $\boldsymbol{d}_{\boldsymbol{k}} \times \boldsymbol{d}^*_{\boldsymbol{k}} = 0$).

The Hamiltonian in each superconductor is described by

$$\mathcal{H}_j = \sum_{\boldsymbol{k}} \Psi^\dagger_j(\boldsymbol{k})\, H_j(\boldsymbol{k})\, \Psi_j(\boldsymbol{k}), \tag{6}$$

$$H_j(\boldsymbol{k}) = \begin{bmatrix} \hat{H}_{\mathrm{N}}(j, \boldsymbol{k}) & \hat{\Delta}(j, \boldsymbol{k}) \\ -\undertilde{\hat{\Delta}}(j, \boldsymbol{k}) & -\undertilde{\hat{H}}_{\mathrm{N}}(j, \boldsymbol{k}) \end{bmatrix}, \tag{7}$$

$$\Psi_j(\boldsymbol{k}) = [c_{j,\boldsymbol{k},\uparrow}, c_{j,\boldsymbol{k},\downarrow}, c^\dagger_{j,-\boldsymbol{k},\uparrow}, c^\dagger_{j,-\boldsymbol{k},\downarrow}]^{\mathrm{T}}, \tag{8}$$

for $j = s$ and t, where $c_{j,\boldsymbol{k},\sigma}$ is the annihilation operator of an electron with a wavenumber $\boldsymbol{k}$ and spin σ in a SC labeled by j. Particle-hole conjugation is denoted by $\undertilde{X}(\boldsymbol{k}, \omega_n) \equiv X^*(-\boldsymbol{k}, \omega_n)$. The Green's function in each SC is calculated as a solution of the Gor'kov equation,

$$[i\omega_n - H_j(\boldsymbol{k})] \begin{bmatrix} \hat{G}_j(\boldsymbol{k}, \omega_n) & \hat{F}_j(\boldsymbol{k}, \omega_n) \\ -\undertilde{\hat{F}}_j(\boldsymbol{k}, \omega_n) & -\undertilde{\hat{G}}_j(\boldsymbol{k}, \omega_n) \end{bmatrix} = 1_{4\times 4}, \tag{9}$$

where $\omega_n = (2n + 1)\pi T$ is the fermionic Matsubara frequency with T being a temperature. The coupling between the two SCs is described phenomenologically by a tunnel Hamiltonian

$$\mathcal{H}_T = \sum_{\boldsymbol{k},\boldsymbol{p},\sigma} \left[-t_{\boldsymbol{k},\boldsymbol{p}}\, c^\dagger_{t,\boldsymbol{k},\sigma}\, c_{s,\boldsymbol{p},\sigma} - t_{\boldsymbol{k},\boldsymbol{p}}\, c^\dagger_{s,\boldsymbol{p},\sigma}\, c_{t,\boldsymbol{k},\sigma} \right]. \tag{10}$$

Within the linear response, the Josephson current between the two SCs is calculated as [23]

$$J = -2e\,T \sum_{\omega_n} \sum_{\boldsymbol{k},\boldsymbol{p}} \mathrm{Im}\,\mathrm{Tr} \left[t_{\boldsymbol{k},\boldsymbol{p}}\, \hat{F}_s(\boldsymbol{p})\, t_{-\boldsymbol{k},-\boldsymbol{p}}\, \undertilde{\hat{F}}_t(\boldsymbol{k}) \right] \tag{11}$$

III. CURRENT

The anomalous Green's function is calculated as

$$\hat{F}_s(\boldsymbol{k}, \omega_n) = -\frac{(\omega_n^2 + \xi^2_{s,\boldsymbol{k}} + |\Delta_{\boldsymbol{k}}|^2 + \boldsymbol{\alpha}^2_{\boldsymbol{k}}) + 2\xi_{s,\boldsymbol{k}} \boldsymbol{\alpha}_{\boldsymbol{k}} \cdot \hat{\boldsymbol{\sigma}}}{Z_s} \times \Delta_{\boldsymbol{k}}\, i\hat{\sigma}_y\, e^{i\varphi_s}, \tag{12}$$

$$Z_s = (\omega_n^2 + \xi^2_{s,\boldsymbol{k}} + |\Delta_{\boldsymbol{k}}|^2 + \boldsymbol{\alpha}^2_{\boldsymbol{k}})^2 - 4\xi^2_{s,\boldsymbol{k}}\, \boldsymbol{\alpha}^2_{\boldsymbol{k}}, \tag{13}$$

in a spin-singlet SC. The first four terms in the numerator of Eq. (12) represent a spin-singlet pairing correlation that is linked to the pair potential through the gap equation in the presence of an attractive interaction between two electrons. The last term describes a spin-triplet odd-parity pairing correlation induced by the SOI. The results in a spin-triplet SC are given by

$$\begin{aligned} \hat{F}_t(\boldsymbol{k}, \omega_n) = &-\frac{1}{Z_t} \left[(\omega_n^2 + \xi^2_{s,\boldsymbol{k}} + |\boldsymbol{d}_{\boldsymbol{k}}|^2 - \boldsymbol{\alpha}^2_{\boldsymbol{k}}) \boldsymbol{d}_{\boldsymbol{k}} \cdot \hat{\boldsymbol{\sigma}} \right. \\ &+ 2(\boldsymbol{\alpha}_{\boldsymbol{k}} \cdot \boldsymbol{d}_{\boldsymbol{k}}) \boldsymbol{\alpha}_{\boldsymbol{k}} \cdot \hat{\boldsymbol{\sigma}} + 2\omega_n (\alpha_{\boldsymbol{k}} \times \boldsymbol{d}_{\boldsymbol{k}}) \cdot \hat{\boldsymbol{\sigma}} \\ &\left. - 2\, \xi_{t,\boldsymbol{k}}\, \boldsymbol{\alpha}_{\boldsymbol{k}} \cdot \boldsymbol{d}_{\boldsymbol{k}} \right] i\, \hat{\sigma}_y\, e^{i\varphi_t}, \end{aligned} \tag{14}$$

$$\begin{aligned} Z_t = &(\omega_n^2 + \xi^2_{t,\boldsymbol{k}} + |\boldsymbol{d}_{\boldsymbol{k}}|^2 + \boldsymbol{\alpha}^2_{\boldsymbol{k}})^2 - 4\xi^2_{t,\boldsymbol{k}}\, \boldsymbol{\alpha}^2_{\boldsymbol{k}} \\ &- 4|\boldsymbol{\alpha}_{\boldsymbol{k}} \times \boldsymbol{d}_{\boldsymbol{k}}|^2. \end{aligned} \tag{15}$$

The first line in Eq. (14) represents a spin-triplet pairing correlation linked to the pair potential. The SOI generates three extra pairing correlations. The first term in the second line describes such a spin-triplet odd-parity pairing correlation. The pairing correlation at the second term in the second line belongs to odd-frequency spin-triplet even-parity symmetry class. The last term describes a spin-singlet even-parity pairing correlation. The spin-singlet and spin-triplet mixed states are realized in the two SCs, which enables the lowest order Josephson coupling between them.

At low temperatures, the tunnel Hamiltonian Eq. (10) works only on electrons at the Fermi level. The wavenumber in the current direction is limited to

$$\frac{p_x^2+\boldsymbol{p}_\parallel^2}{2m_s}+\epsilon_s-\mu=0, \quad \frac{k_x^2+\boldsymbol{k}_\parallel^2}{2m_t}+\epsilon_t-\mu=0, \tag{16}$$

where $\boldsymbol{p}_\parallel$ ($\boldsymbol{k}_\parallel$) is the wavenumber in the yz plane on the Fermi surface at a singlet (triplet) SC. The Fermi wave number is defined by $k_{F,j}=\sqrt{2m_j(\mu-\epsilon_j)}$ for $j=s$ and t. As a result of translational symmetry in the yz plane, the wavenumber in the parallel directions to the plane is preserved in the tunnel process,

$$\boldsymbol{p}_\parallel=\boldsymbol{k}_\parallel. \tag{17}$$

Namely, the tunneling event happens between the states on the Fermi surface at $(\pm p_x, \boldsymbol{k}_\parallel)$ in a spin-singlet SC and those at $(\pm k_x, \boldsymbol{k}_\parallel)$ in a spin-triplet SC. In what follows, we assume that the tunneling amplitude is a constant independent of wavenumber, (i. e., $t_{\boldsymbol{k},\boldsymbol{p}}=t\,\delta_{\boldsymbol{k}_\parallel,\boldsymbol{p}_\parallel}$.) The summation over the wavenumber is expressed as

$$\sum_{\boldsymbol{k}} F(\xi_{\boldsymbol{k}},\hat{\Delta}_{\boldsymbol{k}}) \to \int d\xi_j N(\xi_j)\left\langle F(\xi_j,\hat{\Delta}_{\boldsymbol{k}})\right\rangle_{\bar{\boldsymbol{k}}_\parallel}, \tag{18}$$

$$\left\langle F(\xi_j,\hat{\Delta}_{\boldsymbol{k}})\right\rangle_{\bar{\boldsymbol{k}}_\parallel} = \frac{1}{\pi}\int_0^\pi d\theta \sin^2\theta \int_{-\pi/2}^{\pi/2} d\phi\cos\phi \times F(\xi_j,\hat{\Delta}_{k_x,\boldsymbol{k}_\parallel}), \tag{19}$$

where $N(\xi_j)$ is the density of states per spin. The wavenumber on the Fermi surface is parameterized as $k_x = k_{F,j}\sin\theta\,\cos\phi$, $k_y = k_{F,j}\sin\theta\,\sin\phi$, and $k_z = k_{F,j}\cos\theta$. $\langle\cdots\rangle$ in Eq. (19) means the summation over the propagating channels on the Fermi surface with $k_x > 0$, where $\boldsymbol{k}_\parallel = k_y\bar{\boldsymbol{y}}+k_z\,\bar{\boldsymbol{z}}$, $\bar{\boldsymbol{k}}_\parallel=\boldsymbol{k}_\parallel/k_{F,j}$, and $\bar{\boldsymbol{y}}$ ($\bar{\boldsymbol{z}}$) is the unit vector in the y (z) direction.

The Josephson current is expressed by

$$J = \frac{\pi}{eR_{\mathrm{N}}}T\sum_{\omega_n}\mathrm{Im} \times\left\langle \frac{e^{i\varphi}\,\delta_{\boldsymbol{k}_\parallel,\boldsymbol{p}_\parallel}\,(X_t-X_s)\Delta_{\boldsymbol{p}}}{\sqrt{\omega_n^2+|\Delta_{\boldsymbol{p}}|^2}\sqrt{\omega_n^2+|\boldsymbol{d}_{\boldsymbol{k}}|^2}}\frac{\boldsymbol{\alpha}_{\boldsymbol{k}}\cdot\boldsymbol{d}_{\boldsymbol{k}}^*}{|\boldsymbol{\alpha}_{\boldsymbol{k}}|}\right\rangle_{\bar{\boldsymbol{k}}_\parallel}, \tag{20}$$

with

$$R_{\mathrm{N}}^{-1} = 4\pi e^2t^2\,N_s(0)\,N_t(0), \quad \varphi=\varphi_s-\varphi_t \tag{21}$$

$$X_j = \frac{|\boldsymbol{\alpha}_{\boldsymbol{k}}|}{N_j(0)}\left.\frac{dN_j(\xi_j)}{d\xi_j}\right|_{\xi_j=0} \approx \frac{\lambda k_{F,j}}{\mu-\epsilon_j} \ll 1, \tag{22}$$

for $j=s$ and t, where R_{N} is the resistance of the junction in the normal state. In Appendix, we discuss how to derive Eq. (20). Eq. (20) represents the Josephson current due to the coupling between the pair potential and the induced pairing correlations by Rashba SOI. As the induced spin-triplet component in Eq. (12) is proportional to ξ_s, the Josephson current due to such coupling is proportional to X_s in Eq. (20). The energy derivative of the density of states determines the amplitude of the Josephson current. In the similar way, the coupling between the induced spin-singlet correlation in a spin-triplet SC and the spin-singlet pair potential $\Delta_{\boldsymbol{p}}$ carries the Josephson current proportional to X_t in Eq. (20). The amplitude of the Josephson current at zero temperature is roughly estimated as X_jJ_0, where J_0 in Eq. (A8) is the amplitude of the critical current in the Ambegaokar-Baratoff formula.[24]

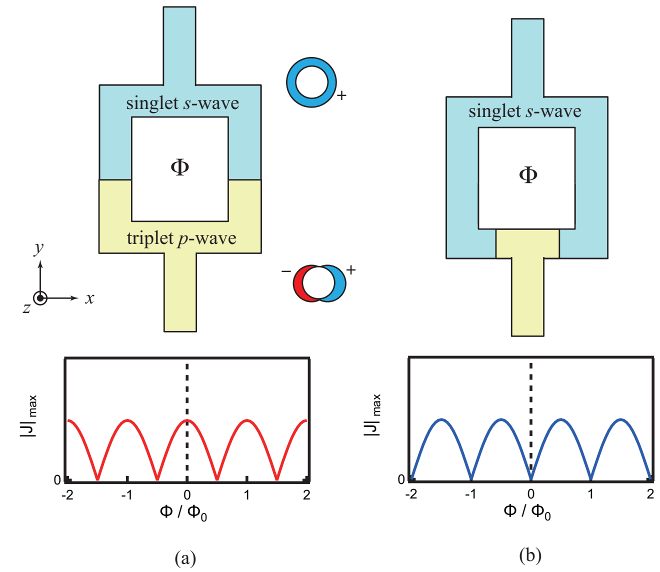

FIG. 2. Schematic picture of two SQUIDs and expected interference patterns. We consider a conventional s-wave pair potential in a spin-singlet superconductor. The interference pattern in (b) is observed only when $\boldsymbol{d}_{\boldsymbol{k}}$ has a component proportional to k_x and the component forms the Josephson coupling. The images of the pair potentials are also illustrated on a two-dimensional Fermi surface.

The results in Eq. (20) also tell us the current-phase relationship (CPR). When both $\Delta_{\boldsymbol{k}}$ and $\boldsymbol{d}_{\boldsymbol{k}}$ are real number, the CPR is sinusoidal as $J\propto\sin\varphi$. For chiral states such as chiral d-wave $\Delta_{\boldsymbol{k}}\propto(k_x+ik_y)k_z$ and chiral p-wave $\boldsymbol{d}_{\boldsymbol{k}}\propto k_x+ik_y$, the CPR may deviate from the sinusoidal function.

IV. SELECTION RULES

A singlet/triplet junction is usually used as a symmetry tester of a spin-triplet SC. Therefore, conventional superconductors such as Nb, Al, and Pb are adopted at a spin-singlet segment. The Josephson current in such a junction becomes

$$J = J_0 \frac{2\Delta}{\Delta_0} T \sum_{\omega_n} \mathrm{Im}\, e^{i\varphi} \frac{X_t - X_s}{\sqrt{\omega_n^2 + \Delta^2}} \times \left\langle \frac{1}{\sqrt{\omega_n^2 + |\boldsymbol{d}_{\boldsymbol{k}}|^2}} \frac{k_y\, d_x^*(\boldsymbol{k}) - k_x\, d_y^*(\boldsymbol{k})}{\sqrt{k_x^2 + k_y^2}} \right\rangle_{\bar{\boldsymbol{k}}_\parallel} . \quad (23)$$

The results imply the selection rules for two parts of $\boldsymbol{d}_{\boldsymbol{k}}$: spin part and orbital part. The Rashba SOI does not couple to the z component of $\boldsymbol{d}_{\boldsymbol{k}}$ that represents a spin-triplet Cooper pair with its spin polarizing in the xy plane. The selection rules for the orbital part are derived from the average over $\boldsymbol{k}_\parallel = k_y \bar{\boldsymbol{y}} + k_z \bar{\boldsymbol{z}}$. The x component of $\boldsymbol{d}_{\boldsymbol{k}}$ must be an odd function of k_y for the average in Eq. (23) being a nonzero value. In the same manner, d_y must be an even function of $\boldsymbol{k}_\parallel$ for a finite Josephson coupling under the odd-parity condition $\boldsymbol{d}_{\boldsymbol{k}} = -\boldsymbol{d}_{-\boldsymbol{k}}$. The selection rules due to Rashba SOI are summarized in the first column from the left in Table I.

For comparison, we briefly derive the selection rules due to SOI at the junction interface proposed by Millis et. al. [22]. The SOI originates from breaking inversion symmetry in the x direction at the junction interface. Therefore, electronic structures in the two SCs must be different from each other [25], (i.e. $m_s \neq m_t$ and/or $\epsilon_s \neq \epsilon_t$). The interface SOI is described by

$$H_I = \lambda_I (\nabla V(\boldsymbol{r})) \times \hat{\boldsymbol{\sigma}} \cdot \boldsymbol{k}, \quad (24)$$

where $V(\boldsymbol{r})$ is the potential barrier at the interface. For the current flowing in the x direction, the Josephson current with $\nabla V(\boldsymbol{r}) \parallel \boldsymbol{x}$ and $\boldsymbol{k}_\parallel = k_y \bar{\boldsymbol{y}} + k_z \bar{\boldsymbol{z}}$ is represented as

$$J_I^{(x)} \propto \langle k_z\, d_y^*(\boldsymbol{k}) - k_y\, d_z^*(\boldsymbol{k}) \rangle_{\bar{\boldsymbol{k}}_\parallel} . \quad (25)$$

To have a nonzero Josephson coupling, d_y must be proportional to k_z and/or d_z must be proportional to k_y. The x component of $\boldsymbol{d}_{\boldsymbol{k}}$ does not contribute to the Josephson current. The results are summarized at the interface SOI $\boldsymbol{j} \parallel \boldsymbol{x}$ in Table I.

The selection rules for the interface SOI depends on the current direction. For the current in the y direction the Josephson current with $\nabla V(\boldsymbol{r}) \parallel \boldsymbol{y}$ and $\boldsymbol{k}_\parallel = k_x \bar{\boldsymbol{x}} + k_z \bar{\boldsymbol{z}}$ is calculated as

$$J_I^{(y)} \propto \langle k_z\, d_x^*(\boldsymbol{k}) - k_x\, d_z^*(\boldsymbol{k}) \rangle_{\bar{\boldsymbol{k}}_\parallel} . \quad (26)$$

The y component of $\boldsymbol{d}_{\boldsymbol{k}}$ does not contribute to the Josephson current. The relations $d_x \propto k_z$ and/or $d_z \propto k_x$ are necessary for the lowest order Josephson coupling. Eq. (24) indicates that the Josephson current due to the interface SOI for the current in the l direction can be described as

$$J^{(l)} \propto \langle \epsilon_{l,m,n}\, d_m\, k_n \rangle_{\bar{\boldsymbol{k}}_\parallel} , \quad \boldsymbol{k}_\parallel = k_n \bar{\boldsymbol{n}} + k_m \bar{\boldsymbol{m}}, \quad (27)$$

where $\epsilon_{l,m,n}$ are the antisymmetric tensors. Therefore, $\boldsymbol{d}_{\boldsymbol{k}}$ proportional to k_l do not contribute to the Josephson coupling.

TABLE I. The selection rules for $\boldsymbol{d}_{\boldsymbol{k}}$ are summarized for the lowest order Josephson coupling. For the Rashba SOI, the Josephson current flows when $\boldsymbol{d}_{\boldsymbol{k}}$ has a component of $d_x \propto k_y$ as indicated at the first row and/or $d_y \propto k_x$ as indicated at the second row. At the first row, the presence of $d_x \propto k_y$ gives the interference pattern in Fig. 2(a) as shown by "$\circ$". But it does not explain the interference pattern in Fig. 2(b) as shown by "$\times$". At the second row, the presence of $d_y \propto k_x$ explain successfully the both interference patters in Fig. 2. The Rashba SOI does not couple to the z component of $\boldsymbol{d}_{\boldsymbol{k}}$. The selection rules due to the interface SOI in Eq. (24) [22] are also shown. The interface SOI cannot give the Josephson coupling that reproduces the interference pattern in Fig. 2(b).

pair potential	Fig. 2(a)	Fig. 2(b)
Rashba SOI		
$d_x(\boldsymbol{k}) \propto k_y$	$\circ$	$\times$
$d_y(\boldsymbol{k}) \propto k_x$	$\circ$	$\circ$
$d_z(\boldsymbol{k})$ no coupling	$\times$	$\times$
Interface SOI $\boldsymbol{j} \parallel \boldsymbol{x}$		
$d_x(\boldsymbol{k})$ no coupling	$-$	$\times$
$d_y(\boldsymbol{k}) \propto k_z$	$-$	$\times$
$d_z(\boldsymbol{k}) \propto k_y$	$-$	$\times$
Interface SOI $\boldsymbol{j} \parallel \boldsymbol{y}$		
$d_x(\boldsymbol{k}) \propto k_z$	$\circ$	$-$
$d_y(\boldsymbol{k})$ no coupling	$\times$	$-$
$d_z(\boldsymbol{k}) \propto k_x$	$\circ$	$-$

V. EXPERIMENT IN TWO SQUIDS

A previous paper [15] proposed a phase-sensitive experiment to identify a spin-triplet odd-parity SC using two SQUIDs in Fig. 2, where Φ is the magnetic flux through the hole and $\Phi_0 = \pi/e$. When superconducting states are uniform, the two singlet/triplet junctions in Fig. 2(a) are identical to each other irrespective of symmetries in the pair potential. The maximum value of the Josephson current $|J_{\max}|$ takes its maximum at $\Phi = 0$ as shown in the lower panel of Fig. 2(a). Details of the derivation are given in Appendix B, where we assume that the two junctions are 0-junction at $\Phi = 0$ and the CPR is sinusoidal $J = J_{\mathrm{ST}} \sin\varphi$. In a SQUID in Fig. 2(b), the two singlet/triplet junctions are not identical to each other when $\boldsymbol{d}_{\boldsymbol{k}}$ has an odd-parity component proportional to k_x. When one junction is 0-junction, the other becomes π-junction. As a result, $|J_{\max}|$ takes its minimum at $\Phi = 0$ as shown in the lower panel of Fig. 2(b). Thus the difference between the two interference patterns in Fig. 2 could be a direct evidence of spin-triplet odd-parity superconductivity. In particular, the interference pattern in Fig. 2(b) is an essential property of spin-triplet SCs. In this section, we refine these phenomenological arguments by taking into account the selection rules in Table I.

We first discuss the selection rules for the interface SOIs. For a SQUID in Fig. 2(a) with the current in the y direction, the interference pattern in Fig. 2(a) can be explained when $\boldsymbol{d}_{\boldsymbol{k}}$ has the components of $d_x \propto k_z$ and/or $d_z \propto k_x$. At the second column in Table I, "$\circ$" means that the presence of such components reproduces the interference pattern in Fig. 2 (a). Generally speaking, any lowest order singlet/triplet couplings result in the interference pattern in Fig. 2(a). On the other hand, to explain the interference pattern in Fig. 2(b), the SOI is necessary to couple to a component of $\boldsymbol{d}_{\boldsymbol{k}}$ proportional to k_x. The selection rules for the interface SOI with $\boldsymbol{j} \parallel \boldsymbol{x}$ are presented in Table I. At the last column, "$\times$" means that the Josephson coupling due to the interface SOI cannot give the interference pattern in Fig. 2 (b). This conclusion is independent of details of $\boldsymbol{d}_{\boldsymbol{k}}$. Therefore, the phenomenological theory by GLB [15] has required other mechanisms of the singlet/triplet coupling than the interface SOI.

Second, we examine the possibility of the Rashba SOI. The selection rules discussed with Eq. (23) can be applied to the SQUID in Fig. 2(b) because the current flows in the x direction. The Rashba SOI couples to two components: $d_x \propto k_y$ and $d_y \propto k_x$. In the former case, both singlet/triplet junctions in Fig. 2(b) become 0-junction or π-junction simultaneously because $d_x \propto k_y$ is an even function of k_x. Thus such coupling cannot explain the interference pattern in Fig. 2(b) as indicated by $\times$ at the last column in Table. I. On the other hand, the latter $d_y \propto k_x$ is an odd function of k_x. As a result, one singlet/triplet junction in Fig. 2(b) becomes π-junction and the other 0-junction, which explains the interference pattern in Fig. 2(b) as indicated by $\circ$ in Table I. The results for a SQUID in Fig. 2(a) are derived by considering $\boldsymbol{k}_\parallel = k_x\bar{\boldsymbol{x}} + k_z\bar{\boldsymbol{z}}$ because the current flows in the y direction. It is easy to confirm that the first column in Table. I remains unchanged and both of $d_x \propto k_y$ and $d_y \propto k_x$ give the interference pattern in Fig. 2(a). Thus, the Rashba SOI generates the single/triplet Josephson coupling necessary for the SQUID in Fig. 2(b) to function as a symmetry testing device [15]. The experimental findings [16] strongly suggest that $\boldsymbol{d}_{\boldsymbol{k}}$ in β-Bi_2Pd must has a component of $d_y \propto k_x$. As briefly mentioned in the introduction, characteristic properties of a spin-triplet SC originate from its $\boldsymbol{d}$-vector. The component of $d_y \propto k_x$ can be confirmed by an another junction experiment, where a spin-triplet SC is replaced by a normal metal in Fig. 1. The conclusion $d_y \propto k_x$ suggests that the anomalous proximity effect is expected in the normal metal and that such effect can be confirmed by the conductance spectroscopy in a T-shaped junction [12, 13].

Third, we briefly discuss effects of SOIs in a bulk spin-triplet SC derived from the lattice structures such as Rashba SOI in noncentrosymmetric SCs and Dresselhaus SOI. These SOIs can be a source of anisotropy in the magnetic susceptibility in both the normal and the superconducting states. The current expression in Eq. (20) can be applied to any triplet SCs $\boldsymbol{d}_{\boldsymbol{k}}$ and to any SOIs $\boldsymbol{\alpha}_{\boldsymbol{k}}$. As displayed in Eq. (14), $\langle \boldsymbol{\alpha}_{\boldsymbol{k}} \cdot \boldsymbol{d}_{\boldsymbol{k}} \rangle_{\bar{\boldsymbol{k}}_\parallel} \neq 0$ is a necessary condition for the lowest order Josephson coupling in Fig. 2(b). Therefore, the product $\boldsymbol{\alpha}_{\boldsymbol{k}} \cdot \boldsymbol{d}_{\boldsymbol{k}}$ must be nonzero and an even function of $\boldsymbol{k}_\parallel$. The anomalous Green's function in Eq. (14) has a pairing correlation belonging to odd-frequency symmetry class which is proportional to $\boldsymbol{\alpha}_{\boldsymbol{k}} \times \boldsymbol{d}_{\boldsymbol{k}}$. It has been established that odd-frequency Cooper pairs decrease the transition temperature and make superconducting state unstable [26, 27]. Therefore, $\boldsymbol{d}_{\boldsymbol{k}}$ should be determined self-consistently to minimize the amplitude of odd-frequency pairing correlation and, as a result, maximize the product $\boldsymbol{\alpha}_{\boldsymbol{k}} \cdot \boldsymbol{d}_{\boldsymbol{k}}$. To reproduce the interference pattern in Fig. 2(b), $\boldsymbol{\alpha}_{\boldsymbol{k}} \cdot \boldsymbol{d}_{\boldsymbol{k}}$ must be an odd function of k_x additionally. The most stable state $\boldsymbol{\alpha}_{\boldsymbol{k}} \parallel \boldsymbol{d}_{\boldsymbol{k}}$, however, does not indicate such interference pattern.

TABLE II. Symmetry classification of the pair potentials for multi-band/orbital superconductors.

spin	momentum-parity	band-parity
singlet	even	even
triplet	odd	even
singlet	odd	odd
triplet	even	odd

Finally, we consider a possibility of an exotic superconducting state in β-Bi_2Pd. Because of the complicated electronic structures at the Fermi level, β-Bi_2Pd may be a multi-band/orbital SC [17]. The symmetry classification of order parameters in the presence of such an extra internal degree of freedom is shown in Table II [28]. The momentum parity represents the widely accepted symmetry options such as even-party s-wave and odd-parity p-wave. When two electrons at the same conduction band form a Cooper pair, such a pair belongs to even-band-parity class. The pairing correlation function remains unchanged (is symmetric) under the permutation of the band indices of two electrons. Therefore, conventional symmetry classes are included in the two rows from the top of the Table. When an electron in one band and an another electron in a different band form a Cooper pair, such a pair is called interband pair. The interband Cooper pairs are classified into two different classes: even-band-parity class and odd-band-parity class. The pairing correlation function of the former (latter) class is symmetric (antisymmetric) under the permutation of two band indices. The two rows from the botom in the Table correspond to the additional symmetry classes of a multi-band SC. Here we discuss how to interpret the experimental findings [16] in the presence of muti-band degree of freedom of an electron. The π-phase shift in the experiment can be explained only by odd-momentum-parity symmetry of the pair potential. The experimental results can be explained if the pair potential in β-Bi_2Pd belongs to spin-singlet odd-momentum-parity odd-band-parity class. At present, odd-band-parity superconductivity is only a toy model in theories [27, 29]. However, the experiment [16] might indicate a signature of an exotic superconductivity.

VI. CONCLUSION

We have studied the effects of Rashba spin-orbit interaction on the lowest order Josephson coupling in a spin-singlet/spin-triplet superconductor junction fabricated on a substrate. The connection between the two superconductors are described by the tunnel Hamiltonian and the Josephson current is calculated by using the linear response theory. We derive selection rules for the spin and orbital parts of the pair potential in a spin-triplet SC. Based on the selection rules obtained theoretically and the interference patterns observed experimentally in a superconducting quantum interference devise, we specify a possible pair potential in β-Bi_2Pd.

Appendix A: Summation over wavenumber

In the Appendix, we explain how to carry out the summation over wavenumber.

Within the linear response, the Josephson current between the two SCs is calculated as [23]

$$J = -2e\,t^2\,T\sum_{\omega_n}\int d\xi_s\,N_s(\xi_s)\int d\xi_t\,N_t(\xi_t)\,\mathrm{Im}\,\mathrm{Tr}\left[\left\langle \hat{F}_s(\xi_s,\Delta_{\boldsymbol{p}})\,\underset{\sim}{\hat{F}}_t(\xi_t,\boldsymbol{d}_{\boldsymbol{k}})\,\delta_{\boldsymbol{k}_\parallel,\boldsymbol{p}_\parallel}\right\rangle_{\bar{\boldsymbol{k}}_\parallel}\right]. \tag{A1}$$

In a spin-singlet SC, the integral over ξ_s is carried out as

$$\begin{aligned}
&\int d\xi_s N_s(\xi_s)\frac{\xi_s^2+\boldsymbol{\alpha}_{\boldsymbol{p}}^2+\Omega_s^2+2\xi_s\boldsymbol{\alpha}_{\boldsymbol{p}}\cdot\hat{\boldsymbol{\sigma}}}{(\xi_s^2+\boldsymbol{\alpha}_{\boldsymbol{p}}^2+\Omega_s^2+2\xi_s|\boldsymbol{\alpha}_{\boldsymbol{p}}|)(\xi_s^2+\boldsymbol{\alpha}_{\boldsymbol{p}}^2+\Omega_s^2-2\xi_s|\boldsymbol{\alpha}_{\boldsymbol{p}}|)},\\
=&\int d\xi_s\left[\frac{N_s(\xi_s)}{(\xi_s-|\boldsymbol{\alpha}_{\boldsymbol{p}}|)^2+\Omega_s^2}+\frac{N_s(\xi_s)}{(\xi_s+|\boldsymbol{\alpha}_{\boldsymbol{p}}|)^2+\Omega_s^2}+\left(\frac{N_s(\xi_s)}{(\xi_s-|\boldsymbol{\alpha}_{\boldsymbol{p}}|)^2+\Omega_s^2}-\frac{N_s(\xi_s)}{(\xi_s+|\boldsymbol{\alpha}_{\boldsymbol{p}}|)^2+\Omega_s^2}\right)\frac{\boldsymbol{\alpha}_{\boldsymbol{p}}\cdot\hat{\boldsymbol{\sigma}}}{|\boldsymbol{\alpha}_{\boldsymbol{p}}|}\right],\\
=&\frac{\pi}{\Omega_s}\left[N_s(|\boldsymbol{\alpha}_{\boldsymbol{p}}|)+N_s(-|\boldsymbol{\alpha}_{\boldsymbol{p}}|)+\{N_s(|\boldsymbol{\alpha}_{\boldsymbol{p}}|)-N_s(-|\boldsymbol{\alpha}_{\boldsymbol{p}}|)\}\frac{\boldsymbol{\alpha}_{\boldsymbol{p}}\cdot\hat{\boldsymbol{\sigma}}}{|\boldsymbol{\alpha}_{\boldsymbol{p}}|}\right]\approx\frac{2\pi N_s(0)}{\Omega_s}\left[1+X_s\frac{\boldsymbol{\alpha}_{\boldsymbol{p}}\cdot\hat{\boldsymbol{\sigma}}}{|\boldsymbol{\alpha}_{\boldsymbol{p}}|}\right],
\end{aligned} \tag{A2}$$

with $\Omega_s=\sqrt{\omega_n^2+|\Delta_{\boldsymbol{p}}|^2}$. As a result, we obtain

$$\int d\xi_s\,N_s(\xi_s)\,\hat{F}_s(\xi_s,\Delta_{\boldsymbol{p}}) = -\frac{\pi N_s(0)}{\sqrt{\omega_n^2+|\Delta_{\boldsymbol{p}}|^2}}\left(1+X_s\frac{\alpha_{\hat{\boldsymbol{p}}}\cdot\hat{\boldsymbol{\sigma}}}{|\boldsymbol{\alpha}_{\hat{\boldsymbol{p}}}|}\right)\Delta_{\boldsymbol{p}}\,e^{i\varphi_s}i\hat{\sigma}_y. \tag{A3}$$

In a spin-triplet SC, the integral over ξ_t is carried out as

$$\int d\xi_t N_t(\xi_t)\frac{(\xi_s^2-\boldsymbol{\alpha}_{\boldsymbol{k}}^2+\Omega_t^2)\boldsymbol{d}_{\boldsymbol{k}}\cdot\hat{\boldsymbol{\sigma}}+2(\boldsymbol{d}_{\boldsymbol{k}}\cdot\boldsymbol{\alpha}_{\boldsymbol{k}})\boldsymbol{\alpha}_{\boldsymbol{k}}\cdot\hat{\boldsymbol{\sigma}}+2\omega_n(\boldsymbol{\alpha}_{\boldsymbol{k}}\times\boldsymbol{d}_{\boldsymbol{k}})\cdot\hat{\boldsymbol{\sigma}}-2\xi_t\boldsymbol{\alpha}_{\boldsymbol{k}}\cdot\boldsymbol{d}_{\boldsymbol{k}}}{\xi_t^4+2\xi_t^2(\Omega_t^2-\alpha_{\boldsymbol{k}}^2)+(\Omega_t^2+\alpha_{\boldsymbol{k}}^2)^2-4|\boldsymbol{\alpha}_{\boldsymbol{k}}\times\boldsymbol{d}_{\boldsymbol{k}}|^2}, \tag{A4}$$

$$\approx\frac{\pi N_t(0)}{\Omega_t}\left[\frac{\Omega_t^2\boldsymbol{d}_{\boldsymbol{k}}\cdot\hat{\boldsymbol{\sigma}}+(\boldsymbol{d}_{\boldsymbol{k}}\cdot\boldsymbol{\alpha}_{\boldsymbol{k}})\boldsymbol{\alpha}_{\boldsymbol{k}}\cdot\hat{\boldsymbol{\sigma}}+\omega_n(\boldsymbol{\alpha}_{\boldsymbol{k}}\times\boldsymbol{d}_{\boldsymbol{k}})\times\hat{\boldsymbol{\sigma}}}{\Omega_t^2+\boldsymbol{\alpha}_{\boldsymbol{k}}^2}+X_t\frac{\boldsymbol{\alpha}_{\boldsymbol{k}}\cdot\boldsymbol{d}_{\boldsymbol{k}}}{|\boldsymbol{\alpha}_{\boldsymbol{k}}|}\right], \tag{A5}$$

with $\Omega_t=\sqrt{\omega_n^2+|\boldsymbol{d}_{\boldsymbol{k}}|^2}$. Here, we neglect $|\boldsymbol{\alpha}_{\boldsymbol{k}}\times\boldsymbol{d}_{\boldsymbol{k}}|^2$ in the denominator of Eq. (A4) to obtain simple expression of the Josephson current. Such approximation change the Josephson current only quantitatively. As a result, we obtain

$$\int d\xi_t\,N_t(\xi_t)\,\underset{\sim}{\hat{F}}_t(\xi_t,\boldsymbol{d}_{\boldsymbol{k}}) = -\frac{\pi N_t(0)}{\Omega_t}i\hat{\sigma}_y\,e^{-i\varphi_t}\left[\boldsymbol{f}_t\cdot\hat{\boldsymbol{\sigma}}+X_t\frac{\boldsymbol{\alpha}_{\boldsymbol{k}}\cdot\boldsymbol{d}_{\boldsymbol{k}}^*}{|\boldsymbol{\alpha}_{\boldsymbol{k}}|}\right], \tag{A6}$$

$$\boldsymbol{f}_t=\frac{\Omega_t^2\boldsymbol{d}_{\boldsymbol{k}}^*+(\boldsymbol{d}_{\boldsymbol{k}}^*\cdot\boldsymbol{\alpha}_{\boldsymbol{k}})\boldsymbol{\alpha}_{\boldsymbol{k}}-\omega_n(\boldsymbol{\alpha}_{\boldsymbol{k}}\times\boldsymbol{d}_{\boldsymbol{k}}^*)}{\Omega_t^2+\boldsymbol{\alpha}_{\boldsymbol{k}}^2}. \tag{A7}$$

By substituting Eqs. (A3) and (A6) into Eq. (A1), we obtain Eq. (20).

For a junction consisting of two identical spin-singlet s-wave superconductors, the Josephson current calculated as

$$J = -2et^2T\sum_{\omega_n}\mathrm{Im}\,\mathrm{Tr}\,e^{i\varphi}\left[\frac{\pi N_s\Delta i\hat{\sigma}_y}{\sqrt{\omega_n^2+\Delta^2}}\right]^2 = J_0\frac{\Delta}{\Delta_0}\tanh\left[\frac{\Delta}{2T}\right],\quad J_0\equiv\frac{\pi\Delta_0}{2eR_{\mathrm{N}}}. \tag{A8}$$

The results recover the Ambegaokar-Baratoff formula,[24] where Δ_0 is the amplitude of the pair potential at zero temperature.

Appendix B: Current in two SQUIDs

Here we summarize an argument in Ref. [15]. The total current flowing in a SQUID in Fig. 2 is described by the summation of the two currents flowing the two arms $J = J_L + J_R$. In Fig. 2(a), the two junctions are equivalent to each other at $\Phi = 0$. Thus the currents are described as

$$J_L = J_{\rm ST} \sin\left(\varphi + \pi \frac{\Phi}{\Phi_0}\right), \tag{B1}$$

$$J_R = J_{\rm ST} \sin\left(\varphi - \pi \frac{\Phi}{\Phi_0}\right), \tag{B2}$$

$$\Phi_0 = \frac{\pi \hbar c}{e}, \tag{B3}$$

where $J_{\rm ST} > 0$ is the the amplitude of the Josephson current in each arm. Since $J = 2J_{\rm ST} \sin\varphi \cos(\pi\Phi/\Phi_0)$, the maximum Josephson current in a SQUID in Fig. 2(a) becomes

$$|J|_{\max} = 2J_{\rm ST} \left|\cos\left(\pi \frac{\Phi}{\Phi_0}\right)\right|, \tag{B4}$$

which takes its maximum at $\Phi = 0$.

On the other hand, a SQUID in Fig. 2(b), the sign change of the pair potential shifts the phase at the left junction by π. Thus the two currents are described as

$$J_L = J_{\rm ST} \sin\left(\varphi + \pi + \pi \frac{\Phi}{\Phi_0}\right), \tag{B5}$$

$$J_R = J_{\rm ST} \sin\left(\varphi - \pi \frac{\Phi}{\Phi_0}\right). \tag{B6}$$

The maximum Josephson current in a SQUID in Fig. 2(b) results in

$$|J|_{\max} = 2J_{\rm ST} \left|\sin\left(\pi \frac{\Phi}{\Phi_0}\right)\right|, \tag{B7}$$

which takes its minimum at $\Phi = 0$. The difference between the interference pattern in the two SQUIDs tells us the odd-parity symmetry of the pair potential.

[1] G. R. Stewart, Z. Fisk, J. O. Willis, and J. L. Smith, Possibility of coexistence of bulk superconductivity and spin fluctuations in UPt_3, Phys. Rev. Lett. **52**, 679 (1984).

[2] H. R. Ott, H. Rudigier, Z. Fisk, and J. L. Smith, Ube_{13}: An unconventional actinide superconductor, Phys. Rev. Lett. **50**, 1595 (1983).

[3] S. S. Saxena, P. Agarwal, K. Ahilan, F. M. Grosche, R. K. W. Haselwimmer, M. J. Steiner, E. Pugh, I. R. Walker, S. R. Julian, P. Monthoux, G. G. Lonzarich, A. Huxley, I. Sheikin, D. Braithwaite, and J. Flouquet, Superconductivity on the border of itinerant-electron ferromagnetism in uge_2, Nature **406**, 587 (2000).

[4] S. Ran, C. Eckberg, Q.-P. Ding, Y. Furukawa, T. Metz, S. R. Saha, I.-L. Liu, M. Zic, H. Kim, J. Paglione, and N. P. Butch, Nearly ferromagnetic spin-triplet superconductivity, Science **365**, 684 (2019).

[5] L. Jiao, S. Howard, S. Ran, Z. Wang, J. Olivares Rodriguez, M. Sigrist, Z. Wang, N. P. Butch, and V. Madhavan, Chiral superconductivity in heavy-fermion metal ute2, Nature **579**, 523 (2020).

[6] Y. S. Hor, A. J. Williams, J. G. Checkelsky, P. Roushan, J. Seo, Q. Xu, H. W. Zandbergen, A. Yazdani, N. P. Ong, and R. J. Cava, Superconductivity in $Cu_xBi_2Se_3$ and its Implications for Pairing in the Undoped Topological Insulator, Phys. Rev. Lett. **104**, 057001 (2010).

[7] S. Sasaki, M. Kriener, K. Segawa, K. Yada, Y. Tanaka, M. Sato, and Y. Ando, Topological Superconductivity in $Cu_xBi_2Se_3$, Phys. Rev. Lett. **107**, 217001 (2011).

[8] M. Sato, Nodal structure of superconductors with time-reversal invariance and Z_2 topological number, Phys. Rev. B **73**, 214502 (2006).

[9] M. Sato and S. Fujimoto, Topological phases of noncentrosymmetric superconductors: Edge states, Majorana fermions, and non-Abelian statistics, Phys. Rev. B **79**, 094504 (2009).

[10] R. M. Lutchyn, J. D. Sau, and S. Das Sarma, Majorana Fermions and a Topological Phase Transition in Semiconductor-Superconductor Heterostructures, Phys. Rev. Lett. **105**, 077001 (2010).

[11] Y. Oreg, G. Refael, and F. von Oppen, Helical Liquids and Majorana Bound States in Quantum Wires, Phys. Rev. Lett. **105**, 177002 (2010).

[12] Y. Asano, Y. Tanaka, A. A. Golubov, and S. Kashiwaya, Conductance spectroscopy of spin-triplet superconductors, Phys. Rev. Lett. **99**, 067005 (2007).

[13] S.-P. Chiu, C. C. Tsuei, S.-S. Yeh, F.-C. Zhang, S. Kirchner, and J.-J. Lin, Observation of triplet superconductivity in $CoSi_2/TiSi_2$ heterostructures, Science Advances **7**, eabg6569 (2021), https://www.science.org/doi/pdf/10.1126/sciadv.abg6569.

[14] Y. Asano, A. A. Golubov, Y. V. Fominov, and Y. Tanaka, Unconventional Surface Impedance of a Normal-Metal Film Covering a Spin-Triplet Superconductor Due to Odd-Frequency Cooper Pairs, Phys. Rev. Lett. **107**, 087001 (2011).

[15] V. B. Geshkenbein, A. I. Larkin, and A. Barone, Vortices with half magnetic flux quanta in "heavy-fermion" superconductors, Phys. Rev. B **36**, 235 (1987).

[16] X. Xu, Y. Li, and C. L. Chien, Observation of odd-parity superconductivity with the geshkenbein-larkin-barone composite rings, Phys. Rev. Lett. **132**, 056001 (2024).

[17] Y. Imai, F. Nabeshima, T. Yoshinaka, K. Miyatani, R. Kondo, S. Komiya, I. Tsukada, and A. Maeda, Superconductivity at 5.4 K in $\beta - Bi_2Pd$, Journal of the Physical Society of Japan **81**, 113708 (2012), https://doi.org/10.1143/JPSJ.81.113708.

[18] M. Sakano, K. Okawa, M. Kanou, H. Sanjo, T. Okuda, T. Sasagawa, and K. Ishizaka, Topologically protected surface states in a centrosymmetric superconductor $\beta - PdBi_2$, Nature Communications **6**, 8595 (2015).

[19] Y. Li, X. Xu, M.-H. Lee, M.-W. Chu, and C. L. Chien, Observation of half-quantum flux in the unconventional superconductor β-bi2pd, Science **366**, 238 (2019), https://www.science.org/doi/pdf/10.1126/science.aau6539.

[20] L. P. Pitaevskii and W. P. Halprin, eds., *Helium Three (Modern Problems in Condensed Matter Sciences)* (North Holland, 1990).

[21] T. Shishidou, H. G. Suh, P. M. R. Brydon, M. Weinert,

and D. F. Agterberg, Topological band and superconductivity in UTe_2, Phys. Rev. B **103**, 104504 (2021).

[22] A. Millis, D. Rainer, and J. A. Sauls, Quasiclassical theory of superconductivity near magnetically active interfaces, Phys. Rev. B **38**, 4504 (1988).

[23] G. D. Mahan, *Many-Particle Physics* (Plenum Press, New York, 1990).

[24] V. Ambegaokar and A. Baratoff, Tunneling Between Superconductors, Phys. Rev. Lett. **10**, 486 (1963).

[25] Y. Asano, Y. Tanaka, M. Sigrist, and S. Kashiwaya, Josephson current in s-wave-superconductor/$\mathrm{sr}_2\mathrm{ruo}_4$ junctions, Phys. Rev. B **67**, 184505 (2003).

[26] Y. Asano and A. Sasaki, Odd-frequency Cooper pairs in two-band superconductors and their magnetic response, Phys. Rev. B **92**, 224508 (2015).

[27] T. Sato, S. Kobayashi, and Y. Asano, Discontinuous transition to a superconducting phase, Phys. Rev. B **110**, 144503 (2024).

[28] A. M. Black-Schaffer and A. V. Balatsky, Odd-frequency superconducting pairing in multiband superconductors, Phys. Rev. B **88**, 104514 (2013).

[29] M. Gomes da Silva, F. Dinóla Neto, I. Padilha, J. Ricardo de Sousa, and M. Continentino, First-order superconducting transition in the inter-band model, Physics Letters A **378**, 1396 (2014).